Review

Carbon-Supported PtRuMo Electrocatalysts for Direct Alcohol Fuel Cells

María V. Martínez-Huerta [1],*, Nikolaos Tsiouvaras [1], Gonzalo García [1,2], Miguel A. Peña [1], Elena Pastor[2], José L. Rodriguez [2] and José L.G. Fierro [1]

[1] Instituto de Catálisis y Petroleoquímica, Consejo Superior de Investigaciones científicas (CSIC), c/ Marie Curie, 2. 28049 Madrid, Spain; E-Mails: nikos.tsiouvaras@gmail.com (N.T.); gonau111@gmail.com (G.G.); mapena@icp.csic.es (M.A.P.); jlgfierro@icp.csic.es (J.L.G.F.)

[2] Instituto Universitario de Materiales y Nanotecnología, Departamento de Química Física, Universidad de La Laguna, 38071-La Laguna, Tenerife, Spain; E-Mails: epastor@ull.es (E.P.); jlrguez@ull.es (J.L.R.)

* Author to whom correspondence should be addressed; E-Mail: mmartinez@icp.csic.es; Tel.: +34-91-585-4787; Fax: +34-91-585-4760.

Abstract: The review article discusses the current status and recent findings of our investigations on the synthesis and characterization of carbon-supported PtRuMo electrocatalysts for direct alcohol fuel cells. In particular, the effect of the carbon support and the composition on the structure, stability and the activity of the PtRuMo nanoparticles for the electrooxidation of CO, methanol and ethanol have been studied. Different physicochemical techniques have been employed for the analysis of the catalysts structures: X-ray analytical methods (XRD, XPS, TXRF), thermogravimetry (TGA) and transmission electron microscopy (TEM), as well as a number of electrochemical techniques like CO adsorption studies, current-time curves and cyclic voltammetry measurements. Furthermore, spectroscopic methods adapted to the electrochemical systems for *in situ* studies, such as Fourier transform infrared spectroscopy (FTIRS) and differential electrochemical mass spectrometry (DEMS), have been used to evaluate the oxidation process of CO, methanol and ethanol over the carbon-supported PtRuMo electrocatalysts.

Keywords: electrocatalysts; direct methanol fuel cells; DMFC; CO; methanol; ethanol; PtRuMo; ternary catalysts

1. Introduction

Fuel cells fed with methanol (CH_3OH) or ethanol (C_2H_5OH), in the form of direct alcohol fuel cells (DAFCs) and using a proton-exchange membrane, are being considered as alternatives to hydrogen [1,2]. The main advantage of both alcohols is that they are liquid, and therefore, the storage problems when hydrogen is used are solved. Additionally, the power density of the alcohols in terms of energy by volume of fuel is much higher at standard conditions. When comparing methanol and ethanol fuels, the attention is focused on the use of methanol because of its better reaction kinetics, and hence, better performance in direct methanol fuel cells. Nevertheless, ethanol has received considerable interest due to its low toxicity and because it can be produced in large amounts as renewable biofuel from the fermentation of biomass.

Two catalytic processes occur within these fuel cells (Figure 1). At the anode, alcohol is oxidized by releasing electrons and protons (and CO_2), while at the cathode protons, electrons and oxygen are recombined, throughout a catalytic process, producing water. This means that catalysts, in the form of metal nanoparticles, are needed on each side of the cell. However, along with the rapid DAFCs' development, a series of challenging problems have emerged such as low alcohol electrooxidation kinetics. Therefore, the success of the DAFCs largely depends on the electrocatalysts [3,4].

Figure 1. Schematic representation of the two electrocatalytic processes in a direct alcohol fuel cell.
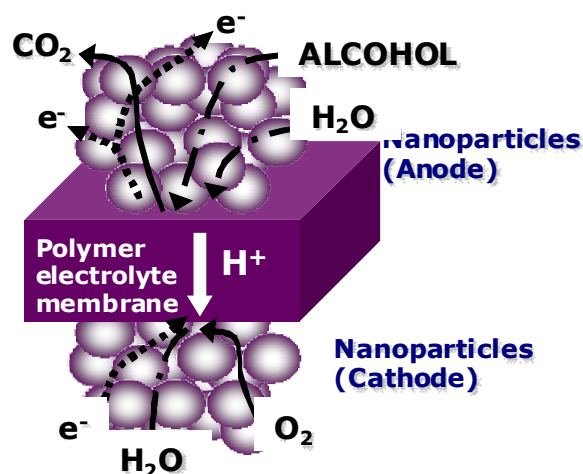
Based on the present development status of the electrocatalysts for methanol and ethanol oxidation, it is recognized that carbon-supported Pt-based catalysts are the most active anode materials for direct alcohol fuel cells. However, pure Pt is readily poisoned by strongly adsorbed intermediates, especially by adsorbed CO. In order to minimize the poisoning effects and to increase the electrocatalytic activity, two or three metals have been added on the surface. Concerning the methanol oxidation, PtRu nanoparticles have shown the best performance among the binary catalysts examined [5–10]. On the other hand, although the full oxidation of ethanol to carbon dioxide has a favorable thermodynamic potential of 0.08 V (*vs.* RHE), the efficiency of direct ethanol fuel cells is already severally limited by the formation of partial oxidation products (containing an intact carbon-carbon bond) and strongly adsorbed intermediates. The great body of work developed in the last few years indicates that various Pt-based catalysts such as

PtSn [11–13] or PtRu [14–16] display enhanced electrocatalytic performance for ethanol electrooxidation with respect to monometallic Pt catalyst. In both reactions, the use of oxophilic atoms can aid in the oxidation of CO from the surface as they enhance the activation of water to form surface hydroxides, which can more readily oxidize CO and CH_x intermediates that form via bifunctional pathways [17,18]. In addition to these bifunctional effects, ligand or electronic effects are also thought to be important in Pt-alloys [19].

However, from the practical standpoint in a real fuel cell environment, a high catalyst loading is required in order to achieve acceptable fuel cell performance, especially when considering the lifetime of the fuel cell. At the same time, this highly noble catalyst loading will definitely be costly, hindering the commercialization of DAFCs. Therefore, the reduction of the catalyst loading through further improvement of activity and optimization of catalyst utilization is necessary. Along these lines, two important approaches are being considered: improvement of the mass activity of Pt-based catalysts by partial substitution of the noble metal [20] and the development of new carbon supports to provide high surface area, good electrical conductivity, suitable porosity to allow good reactant and product flux, and high stability in fuel cell environments [21].

Ternary electrocatalysts based on carbon supported PtRuMo nanoparticles have attracted major attention in recent years for PEMFCs, fuelled with H_2/CO or low molecular weight alcohols [22–37]. Mo is a cheaper and more abundant transition metal than Pt and Ru. Molybdenum oxide possesses thermodynamic characteristics that allow water discharge at low overpotentials [38]; consequently, the dissociation of water appears to be much easier on the bimetallic PtMo than on the monometallic Pt [39]. Additionally, nonstoichiometric lower valence molybdenum oxides, called the Magneli phases, which have compositions between MoO_2 and MoO_3, have a rutile-type structure with short metal-metal bond distance along the direction of edge sharing, which accounts for the high electronic conductivity of these materials [40].

For the complex trimetallic PtRuMo systems not only their reproducible synthesis but also their systematic structural characterization proved to be difficult. The structural characteristics as compositions, chemical state, type of crystal phases, degree of alloying, particle size and the electrochemical role and stability of Mo are not fully determined. This difficulty comes from the inability to synthesize PtRuMo nanoparticles supported on carbon of a controlled chemical composition and particle size is still complicated. The synthesis methods used can be classified in (i) one-step method or simultaneous incorporation of the three metals [31,33,35–37], and (ii) two-step methods or sequential incorporation of Mo and PtRu nanoparticles [27,32]. While a variety of PtRuMo catalysts have been prepared by one-step methods, the ability to control the size and composition is limited due to the propensity of aggregation of metals at the nanoscale. Therefore, the preparation of these electrocatalysts by using a sequential incorporation of the nanoparticles is presented as an attractive alternative for better control of their structural characteristics.

Accordingly, PtRuMo nanoparticles deposited on carbon substrates were prepared by our research group following a two-step procedure [41], whose main innovation was the incorporation of Pt and Ru on a MoO_x/C system, following the colloidal method developed by Watanabe *et al.* [42]. The present paper discusses the recent findings of our investigations of the synthesis and characterization of carbon-supported PtRuMo electrocatalysts for direct alcohol fuel cells [41,43–48]. In particular, the effect of the carbon support and the composition on the structure, stability and the activity of the PtRuMo nanoparticles for

the electrooxidation of CO, methanol and ethanol have been examined in some detail. Different physicochemical techniques have been employed for the analysis of the catalysts' structure: X-ray analytical methods (XRD, XPS, TXRF), termogravimetry (TGA) and transmission electron microscopy (TEM), as well as a number of electrochemical techniques like CO adsorption studies, current-time transients and cyclic voltammetry measurements. Furthermore, spectroscopic methods adapted to the electrochemical systems for *in situ* studies, such as Fourier transform infrared spectroscopy (FTIRS) and differential electrochemical mass spectrometry (DEMS), have been used to evaluate the oxidation processes of CO, methanol and ethanol over the carbon-supported PtRuMo electrocatalysts.

2. Results and Discussion

2.1. Preparation and Characterization of Carbon Supported PtRuMo Catalysts

In general, the new two-step procedure provides carbon supported PtRuMo nanoparticles in the nanoscale range of 2–4 nm. XRD patterns show the characteristic diffraction lines of Pt fcc with a low degree of crystallinity. Neither peaks of Ru and Mo nor of metal oxide phases were found in any catalysts. From the comparison of the electrochemical response combined with an *ex situ* XPS study of the surface species of PtRuMo, it has been confirmed that Mo is present in the oxidized form in the entire potential window, changing form Mo^{3+} to Mo^{6+} as the potential increases [41,49,50]. The effect of the different Mo precursors used [44] and the thermal treatment of ternary catalysts [45] on the structural characteristics and CO and methanol electro-oxidation was also studied.

2.1.1. Effect of Mo Precursor

Carbon supported PtRuMo nanoparticles for CO and methanol electrooxidation were prepared using different Mo precursors ($MoCl_5$ and $(NH_4)_6Mo_7O_{24}$). Structural parameters of PRMCl, PRMNH and PR samples based on the analysis of TXRF, TEM, XRD and XPS are compiled in Table 1.

Table 1. Effect of Mo precursor. Structural parameters of the samples.

| Catalysts	Average particle size (nm) [a]	Atomic ratio Pt:Ru:Mo		
		Bulk composition [b]	Surface composition [c]	Bulk composition after stability test [b]
PRMCl	3.8 ± 0.5	1:1:0.4	1:1.3:0.4	1:0.24:0.05
PRMNH	3.9 ± 0.5	1:1:1.2	1:1.5:1.3	1:0.35:0.3
PR	3.2 ± 0.5	1:0.9	1:1	1:0.6

[a] From TEM; [b] from TXRF; [c] from XPS.

It was observed that the final composition and homogeneity of the ternary catalysts depend greatly on the precursor used. While similar crystal structures and particle sizes are obtained in both PRMNH and PRMCl electrocatalysts, the use of $MoCl_5$ results in a dramatic loss of Mo, whereas $(NH_4)_6Mo_7O_{24}$ seems to be more stable, and therefore, more suitable for synthesis of PtRuMo nanoparticles. This is due to the fact that there is a strong dependence of Mo on the pH of the solution, and Mo is solubilized as polyanions during the synthesis of MoO_x/C. $MoCl_5$ reacts easily with water to give $MoOCl_3$,

$MoO_2(OH)_2$ and HCl compounds, which decrease the pH to values lower than 2. It is known that different Mo^{6+} species are formed depending on the pH of the solution, and namely, at low pH, water soluble species like $MoO_2(H_2O)_4{}^{2+}$ (pH = 0) and MoO_3xH_2O (pH = 2) are predominant in the system [51].

The nature of metal surface species of the samples was investigated by XPS analysis. The Pt 4f signal doublets in all samples are derived from three pairs of Pt species, which are attributed to metallic Pt^0 nanoparticles (71.6–71.7 eV) (~20%), Pt^{2+} species in PtO and $Pt(OH)_2$-like species (72.7–72.9 eV) (~40%) and Pt^{4+} (74.0–74.9 eV) (~40%) [52]. Similar concentrations of Pt species were found in ternary electrocatalysts, while the contribution of Pt^{4+} decreased in binary catalyst,. The Ru $3p_{3/2}$ signal of samples derives of two species in similar concentrations in all catalysts assigned to Ru^{4+} in anhydrous RuO_2 (463.5–463.7 eV) (~80%) and hydrous amorphous RuO_2 xH_2O species (465.6–466.5 eV) (~20%) [44]. The Mo3d spectra for precursors, MoO_x/C samples and electrocatalysts are showed in Figure 2. For the $MoCl_5$ precursor, the most intense $Mo3d_{5/2}$ line was satisfactorily fitted to two components: a major one at 232.1 eV belonging to Mo^{5+} and a minor one at 232.8 eV associated to Mo^{6+}, originated from hydrolyzed $MoCl_5$ species still present in the $MoCl_5$ precursor, which indeed increases in MoO_x/C ($MoCl_5$). Interestingly, the incorporation of Pt and Ru over MoO_x/C ($MoCl_5$) supports results in a catalyst with only Mo^{5+} species. Besides, the Mo $3d_{5/2}$ line of Mo 3d doublet of the ammonium molybdate displayed a major Mo^{6+} component at 232.8 eV which decreases in MoO_x/C ($(NH_4)_6Mo_7O_{24}$) support and especially during the synthesis of PRMNH. Therefore, the binding energies of Mo3d levels point to the fact that incorporation of PtRu over MoO_x/C ($(NH_4)_6Mo_7O_{24}$) and MoO_x/C ($MoCl_5$) supports generates mainly Mo phases with oxidation states of Mo^{5+} and some contribution of Mo^{6+} in the case of PRMNH. In addition, the Pt:Ru:Mo atomic ratio belonging to the topmost atomic layers, derived from XPS analysis (Table 1), is similar to the bulk ratios calculated from TXRF data, and lower amount of metals on the surface of PRMNH are detected compared with PRMCl catalyst.

Figure 2. Mo_{3d} core-level spectra of precursor (**A**); supports (**B**) and electrocatalysts (**C**). Adapted from Tsiouvaras *et al.* [44].
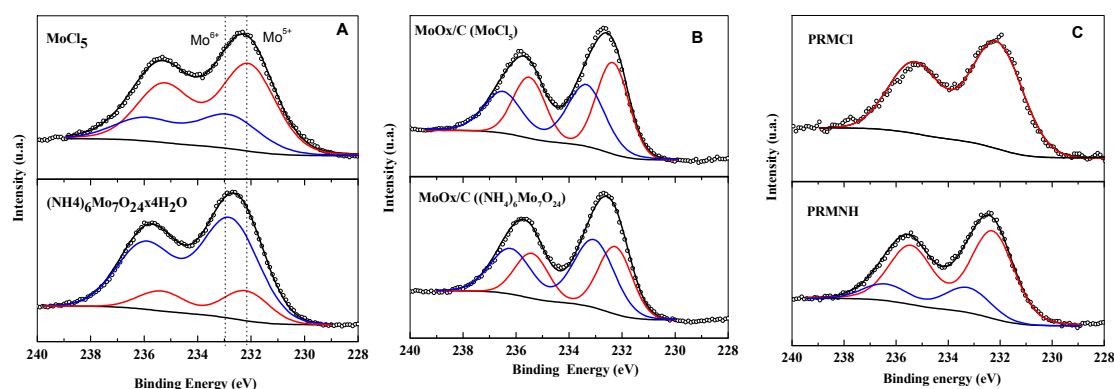
TPR analyses of the MoO_x/C samples are presented in Figure 3 and show different profiles depending on the precursor used. In both samples, the reduction of molybdenum oxides begins at temperatures between 400 and 500 °C. However, different reduction peaks take place at higher temperatures depending on the precursor, where several MoO_x suboxides can be formed. These results

show that the reducibility of supported molybdenum oxides can be altered by the degree of Mo-support chemical interaction and the nature of the surface species developed during preparation of MoO_x/C samples. Incorporation of Pt and Ru shifts the molybdenum oxide reduction peaks at lower temperatures. TPR peaks between 40 and 70 °C in ternary catalysts are due to partially oxidized platinum, and reduction peaks of ca. 100 °C in PR correspond to a RuO_xH_y species [6]. A shift in this reduction peak at higher temperatures in PRMCl (130 °C) and in PRMNH (178 °C) could be due to a direct interaction or a stabilization of oxidation states between Ru and Mo. The other peaks in PRMCl, and PRMNH are assigned to molybdenum oxide species, although the precise phases have not yet been established. Thus, the incorporation of Pt and Ru by the colloidal method can substantially change the coordination of molybdenum oxide, and different MoO_x phases are formed depending on the precursor. Accordingly, the ability of Pt metal nanoparticles to enhance reduction of metal transition oxides by hydrogen via spillover processes is considered [52–54].

Figure 3. Temperature programmed-reduction (TPR) profiles of samples. Adapted from Tsiouvaras *et al.* [44].
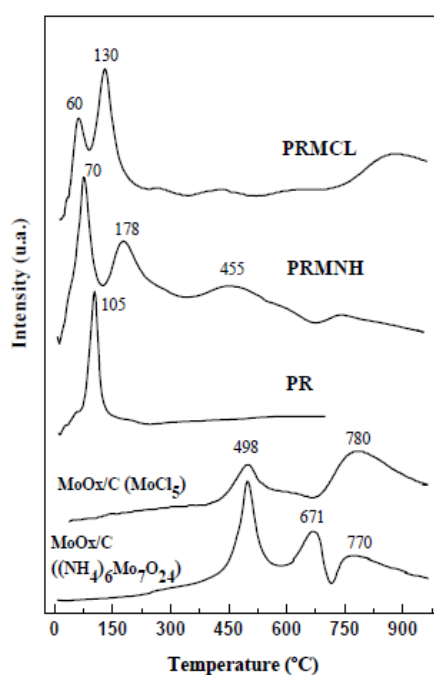
The evolution of the voltammetric profiles of binary and ternary catalysts upon cycling in 0.5 M H_2SO_4 is shown in Figure 4. PR catalyst shows the characteristic cyclic voltammogram of PtRu catalysts without any peak in the 0.25–0.8 V region. The current decrease observed in the curves after several cyclic voltammograms (50 scans) is attributed to some RuO_2 dissolution and some contaminated surface catalyst with sulfito complex. In both ternary systems, a gradual decrease of the peaks between 0.4 and 0.6 V, related to the reduction–oxidation reactions of Mo, is evident, suggesting that Mo dissolves into the electrolyte. The Mo dissolution has also been confirmed in a test by TXRF analysis. When the electrochemical surface of catalysts remained stable under acidic conditions—*i.e.*, the characteristics of the peaks (peak potential, peak height, peak width) do not change after 10 scans—electrocatalysts were removed from the electrode surface and the bulk composition was analyzed. It was observed that ternary catalysts display a dramatic loss of Ru and Mo metals,

especially Mo, while minor loss of Ru was observed in the binary catalyst. It seems that some Ru–Mo interaction take place, which facilitates the Ru dissolution. PRMNH is somewhat the most stable ternary catalyst. Beyond the hydrogen adsorption/desorption region, three apparent oxidation peaks appear at 0.2, 0.45 and 0.6 V in ternary catalysts, though they are less evident in PRMCl. The respective reduction peaks are observed along the cathodic sweep of the voltammograms. Therefore, once the catalysts have been stabilized, similar Mo species along the catalysts' surface tend to remain in all PtRuMo catalysts. That is indicative that similar interactions between metal–support and metal–metal is likely developed in carbon-supported PtRuMo nanoparticles under these potential conditions.

Figure 4. Conventional voltammograms (CV) of electrocatalysts in 0.5 M H_2SO_4 at 25 °C, $v = 0.01$ V s^{-1}. Adapted from Tsiouvaras *et al.* [44].
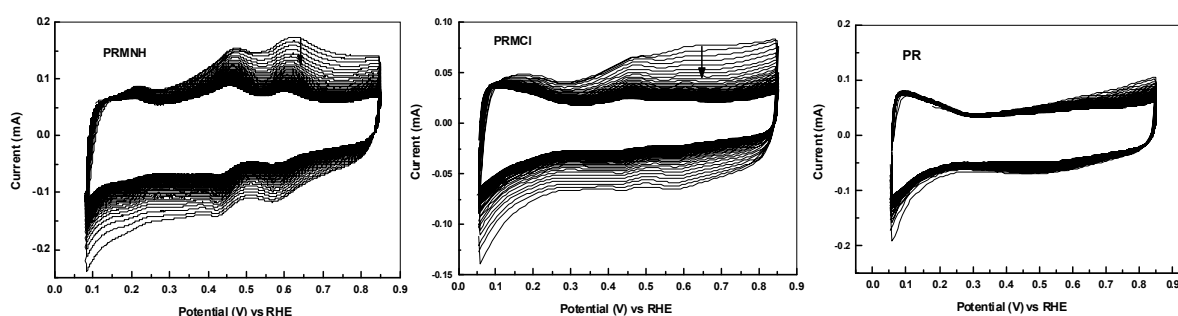

Previous studies on well-defined polycrystalline PtMo alloy electrodes [55] showed that the chemistry of the Mo atoms in the surface (and near surface) is quite complex. Therefore, in the case of ternary PtRuMo catalysts, only a tentative ascription of the peaks is possible allowing qualitative distinction between reduction–oxidation response of Pt, Ru and that of Mo. *In situ* XAS studies were conducted with the aim to identify the nature of surface species of PtMo/C catalysts [56]. The Mo K edge XANES spectra at 0.0 V showed that Mo is present as a hydrated oxide species with an approximated oxidation state of Mo^{5+}, and there is a change in the oxidation state of Mo from Mo^{5+} to Mo^{6+} at 0.54 V, which remains stable till 0.85 V. In our voltammetric results, the redox couple observed at *ca.* 0.2 and 0.45 V do agree with the presence of Mo in an oxidation state between Mo^{5+} and Mo^{6+}. *Ex situ* XPS analyses of electrocatalysts confirm the presence of these species. Unfortunately, no detailed information on the surface composition and its dependence on potential have been reported for PtRuMo catalysts.

The extra peak between 0.60–0.65 V can be explained when the cyclic voltammogram of MoO_x/C support is taken into account (not shown). MoO_x/C voltammogram exhibits one of the major peaks at *ca.* 0.6 V, indicating that non-alloyed carbon supported Mo undergoes a reduction–oxidation reaction in this potential region. Lebedeva and Jansen [57] reported cyclic voltammograms on PtMo/C and Mo/C electrodes interfaced either with H_2SO_4 solutions or with Nafion membrane. They detected an oxidation peak at 0.65 V, which was attributed to isolated Mo species, and another peak at 0.45 V assigned to Mo atoms combined with Pt to form alloyed nanoparticles. This suggests that for all catalysts investigated in the present work some pure non-alloyed Mo—most likely MoO_3 xH_2O—is present on the surface of carbon along with mixed Pt–Mo and/or Ru-Mo phases. Different dissolution rates of the PtRuMo catalysts in a given electrolyte can be related to their homogeneity. As can be seen

from the results (Figure 4) in most cases, the peak at *ca.* 0.6 V decreases quicker than that at *ca.* 0.45 V, suggesting that the non-alloyed MoO_3 phase dissolves more rapidly than Mo from the mixed Pt–MoO_3 phase. Therefore, the stability of a given electrode material is directly related to the degree of mixing of the components, which strongly depends on the salt precursor.

Figure 5. CV for the oxidation of CO in 0.5 M H_2SO_4 at 25 °C of electrocatalysts and the corresponding signal for CO_2 production (m/z = 44), v = 0.01 V s^{-1}. Adapted from Tsiouvaras *et al.* [44].
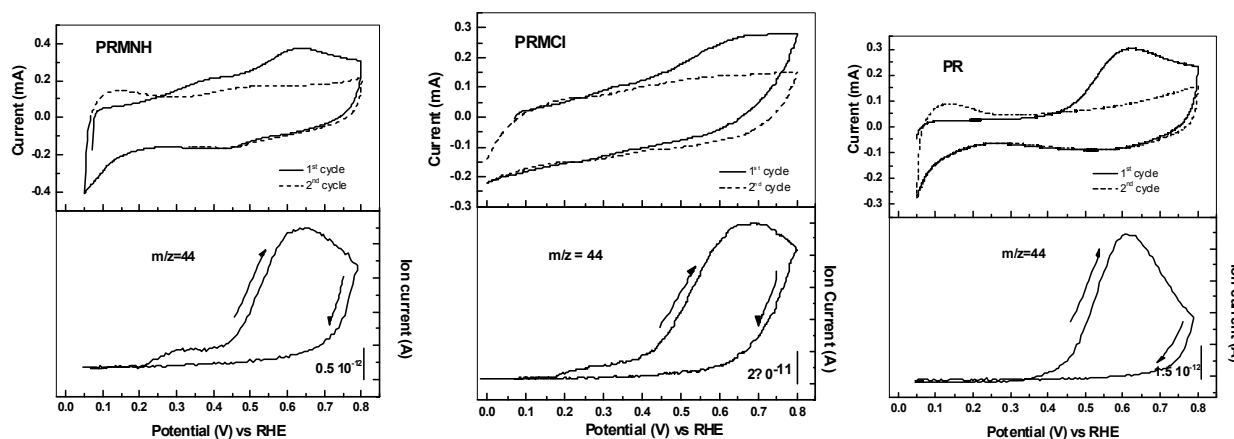
The electrooxidation of CO adsorbed on electrocatalysts (stripping technique) provides information about the activity of the material towards CO oxidation, and the amount of CO oxidized gives information about the active surface area accessible to the reactants, and in some cases, intrinsic catalytic activity towards methanol oxidation. A low onset potential (E_{onset}) for CO oxidation indicates a good CO-tolerance of the electrocatalyst. Exact determination for the onset of CO oxidation reaction from the electrochemical current includes certain difficulties given the need for double-layer correction and sometimes the presence of other faradaic contributions. In this case, differential electrochemical mass spectrometry (DEMS) is more appropriate since no faradaic or double-layer corrections are needed.

Figure 5 depicts the CVs and simultaneously recorded MSCVs related to production of CO_2 (m/z = 44), corresponding to the cation radical $[CO_2]^+$ (DEMS analysis) during the electrooxidation of CO adsorbed on electrocatalysts at 25 °C. The curves indicate that PRMNH and PRMCl catalysts display a high CO tolerance, with the onset for CO_2 production being observed at *ca.* 0.2 V for PRMNH and 0.17 V for PRMCl, which represents a negative shift of about 0.15 V with respect to PR catalyst at the same temperature (E_{onset} = 0.35 V). The shape of the cyclic voltammograms related to production of CO_2 indicates a higher current density at potentials lower than 0.5 V in PRMNH, which implies that CO oxidation occurs easily at the potentials of operation in a PEMFC and DMFC. Current-time curves recorded at 0.6 V in Ar-saturated solution system of 2 M CH_3OH and 0.5 M H_2SO_4 for PRMNH, PRMCl and PR catalyst at 25 °C show better performance of ternary catalyst than the binary system (not shown).

Additionally, PRMNH catalyst displays the best performance compared to the other samples, which corresponds to the superior CO-tolerance of this catalyst. These results confirm that an important,

although not unique, aspect of the catalysis of methanol oxidation is related to catalysis of CO oxidation. Consequently, $(NH_4)_6Mo_7O_{24}$ as the Mo precursor seems to be more stable and handy for synthesis of carbon-supported PtRuMo nanoparticles, it facilitates the Ru-Mo interaction and improves the electrochemical activity towards CO and methanol oxidation.

2.1.2. Effect of Thermal Treatment

The influence of thermal treatment under different environments of PtRuMo/C catalysts was also investigated for CO and methanol electro-oxidation in a half cell and in a DMFC single cell [45]. The thermal treatments of PtRuMo/Vulcan ternary catalyst (labeled PRM) consisted of heating at 300 °C in H_2 (PRMH2) or He atmosphere (PRMHe) for 1 h. Structural parameters are showed in Table 2. The X-ray diffraction patterns of the catalysts (not shown) display diffraction lines of Pt fcc (JPCDS 04802) and the characteristic diffraction pattern of graphitic carbon (24.98°). Neither peaks of Ru and Mo nor of metal oxide phases were found. The heat treatment appears to produce a shift in the Pt (111) peak to a higher diffraction angle. This effect is commonly used to indicate PtRu alloy and it seems that the Mo incorporation improves the PtRu interactions. Lattice parameter has also been calculated in order to evaluate the level of PtRu alloying (Table 2). Results point to the crucial role of the thermal treatment. While the PRM catalyst presents the lattice parameter close to pure Pt (3.920 Å), both types of thermal treatments cause an important reduction of the Pt lattice parameter that is perceived as an improvement in the interaction of Pt-Ru, particularly in PRMH2 (3.894 Å). The Pt-Mo interactions are not visible by this technique since the atomic radii of both metals are very similar and a substitution of Pt atoms in its crystal from Mo atoms would not cause a change in the lattice parameter. TEM results prove that the catalyst treated with H_2 has an average particle size slightly higher (3.7 nm) compared with those obtained for PRM and PRMHe catalysts. In general, a good dispersion with some agglomeration of small particles was observed. Furthermore, TPR and XPS analysis revealed that H_2 treatment provides stronger interactions between Mo and the rest of the metals, and as well a higher amount of Ru in a more reduced oxidation state.

Table 2. Effect of thermal treatment. Structural parameters of the samples.

Catalysts	Pt:Ru:Mo atomic ratio	Average particle size (nm) (TEM)	Lattice parameter (a_{fcc}) (Å)
PRM	1:0.8:0.3	2.5	3.920
PRMHe	1:0.8:0.3	3.2	3.909
PRMH2	1:0.8:0.3	3.7	3.894

The exact onset potential for the CO_{ads} oxidation reaction was accurately evaluated by *in situ* FTIR studies. Other types of electrochemical processes that occur simultaneously like the double layer charge or the adsorption of OH^- oxidizing surface metal atoms can produce current that is very difficult to distinguish from the CO oxidation current. For this reason, *in situ* spectroscopic techniques are important tools to clarify the exact onset potential accurately monitoring the reaction products. In Figure 6, the integrated intensities of the CO_2 bands for the three ternary catalysts as well as the binary PR catalyst and a monometallic 20% Pt catalyst (ETEK) are presented as a function of the potential.

Monometallic catalyst (Pt/C ETEK) was used only as a reference as it contains approximately the same amount of Pt. As it was expected, all ternary catalysts present an onset potential much lower than the homemade binary and the commercial monometallic catalyst. In this study, it is clear that the catalyst thermally treated in H_2 is more tolerant towards CO with the oxidation maximum observed at lower potential. Catalysts PRM and PRMHe seem to be equally tolerant to CO.

Figure 6. Integrated intensities of the CO_2 band for the three ternary catalysts, the home made binary catalyst and the commercial monometallic catalyst 20% Pt/C (ETEK). Adapted from Tsiouvaras *et al.* [45].
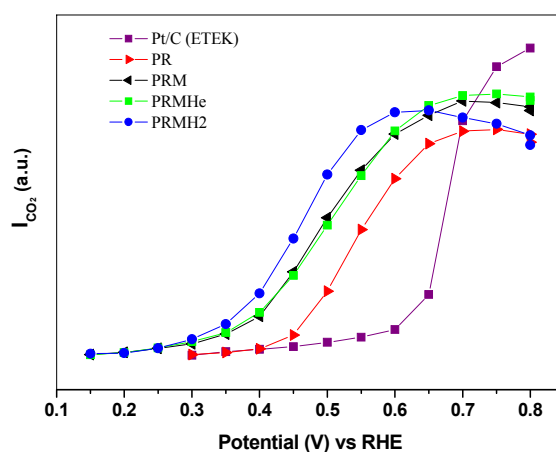

Once MEA was prepared and connected to the single cell; an electrochemical study was conducted in a half cell mode. Anode is the ternary catalyst examined and the cathode is a commercial ETEK (40 wt.% Pt/C catalyst). Both anode and cathode have 2 mg Pt/cm^2. Such a study is identical to the one carried out in the three electrode electrochemical cell. Firstly, the catalyst was activated and stabilized during several cyclic voltammograms between 0.05–0.8 V and once it displayed a repeatable pattern the CO oxidation study begun. As the cell operates at 75 °C, the CO adsorption had to be carried out at a potential lower than the one in a standard CO_{ads} study (0.07 V), in order to make sure that the potential of adsorption is not overlapping with the CO_{ads} oxidation onset potential (E_{onset}). For this reason, and as well for being able to monitor the adsorption, cyclic voltammograms between 0–0.03 V, in the Pt H_2 adsorption area, were performed and the H_2O + CO solution was pumped through the anode until the area of H_2 adsorption was at a minimum (around 30 min). Afterwards the anode was purged from the CO pumping H_2O through it for at least 1 h. In Figure 7, the ternary catalyst PRMH2 is compared to the commercial binary catalyst 30% PtRu/C (JM). As it can be seen, the ternary catalyst presents a much lower oxidation onset than the binary catalyst with a great percentage of the CO_{ads} being oxidized before the potential at which the binary catalysts commences the oxidation (0.3 V). It is obvious that the synergistic effect of Mo is responsible for this oxidation onset, improving remarkably the CO tolerance of the ternary catalysts.

Figure 7. CV of the CO$_{ads}$ oxidation for PRMH2 and commercial catalyst PtRu/C (JM). Experiment performed in a half cell single cell at 75 °C. The continuous line is the first two cycles of the CO$_{ads}$ oxidation of PRMH2, and the dotted line is the first cyclic voltammetry of the CO$_{ads}$ oxidation of the PtRu/C (JM). Adapted from Tsiouvaras *et al.* [45].
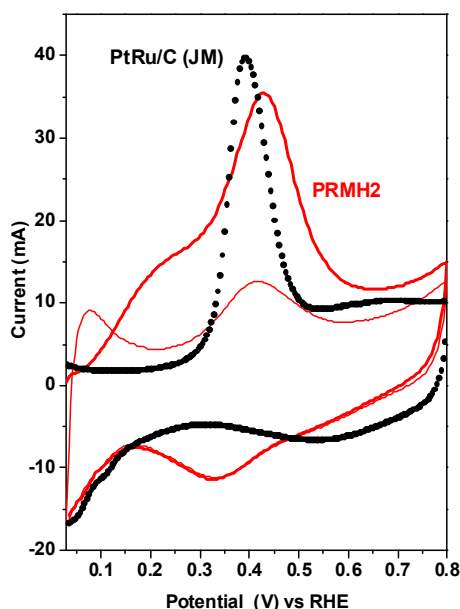
A methanol oxidation study has been carried out in full cell mode. The anode flow is 3.5 cm^3 min^{-1} 2 M CH$_3$OH aqueous solution and the cathode flow is 200 cm^3 min^{-1} synthetic air. Figure 8 compares the performance in activity of the ternary catalysts and it confirms the results obtained in the electrochemical cell. The ternary catalyst treated in H$_2$ is considerably more active than catalysts treated with He or even in the absence of any treatment. Full cell mode was not the normal operation mode for the present experimental setup and this accounts for the relatively low current densities recorded compared with results reported in literature. Nevertheless, the results are reproducible and in good agreement with previous experiments.

Figure 8. Cell voltage *versus* current densities and power densities of a DMFC single cell. Adapted from Tsiouvaras *et al.* [45].
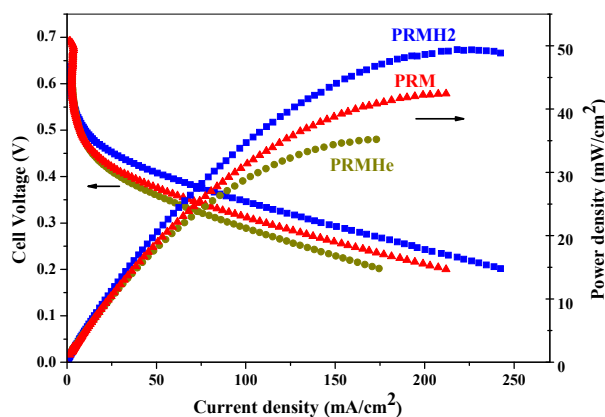
Therefore, thermal treatment with H_2 results in the catalyst being more tolerant towards CO oxidation, and at the same time, it is the most active catalyst towards methanol oxidation. This effect of the thermal treatment is probably related to the improved PtRu alloy that this catalyst presents, but it is as well undoubtedly linked to the presence of Mo as this activation is observed only in ternary catalysts.

2.2. Effect of Carbon Support

Various carbon nanofibers and carbon black (Vulcan XC 72R) were compared as support materials for CO and methanol oxidation PtRuMo catalysts [43]. Carbon nanofibers (NF) are considered as promising support materials for electrocatalyst applications due to their unique properties: resistance to acid/basic media, possibility to control the porosity and surface chemistry, and good electrical and mechanical properties [58]. Carbon nanofibers usually contain a negligible amount of oxygen groups; therefore, in order to study the effect of the surface oxidation on the structure and the electroactivity of the catalysts, the carbon nanofiber was functionalized with HNO_3 (NF.F).

For this study, six catalysts were developed, with three ternary PtRuMo (1:1:1) catalysts: PtRuMo/Vulcan, PtRuMo/NF and PtRuMo/NF.F., and the respective binary PtRu (1:1) counterparts: PtRu/Vulcan, PtRu/NF and PtRu/NF.F. Surface chemistry of carbon nanofibers was studied by TPD experiments (not shown). It was observed that oxidation treatment created a great variety of oxygen surface groups over NF.F (carboxylic, lactones, quinones, phenols and anhydrides groups), whereas they were negligible over NF and carbon Vulcan. The surface chemistry affected to a great extent the incorporation of Mo, and higher Mo lost was observed on the functionalized carbon nanofiber (Table 3). However, PtRuMo/Vulcan and PtRuMo/NF presented a final PtRuMo atomic ratio of 1:0.9:0.7 and 1:0.9:1.2, respectively. Therefore, carbons without oxygen surface groups seemed to be capable of better stabilization of the Mo species. This fact was confirmed by transmission electron microscopy (Figure 9). TEM images of PtRuMo/NF catalyst show a homogeneous distribution of small nanoparticles with some agglomeration of small nanoparticles (Figure 9A), whereas quite heterogeneous distribution was observed on PtRuMo/NF.F (Figure 9 B,C).

Table 3. Effect of support. Structural parameters of the samples.

Catalysts	Bulk composition Pt:Ru (TXRF)	Average particle size (nm) (XRD)	Catalysts	Bulk composition Pt:Ru:Mo (TXRF)	Average particle size (nm) (XRD)
PtRu/Vulcan	1:1	3.1	PtRuMo/Vulcan	1:0.9:0.7	2.6
PtRu/NF	1:0.9	2.5	PtRuMo/NF	1:0.9:1.2	n.d.
PtRu/NF.F	1:0.9	3.4	PtRuMo/NF.F	1:0.8:0.5	3.1

Figure 9. TEM images of PtRuMo/NF (**A**) and PtRuMo/NF.F (**B** and **C**).
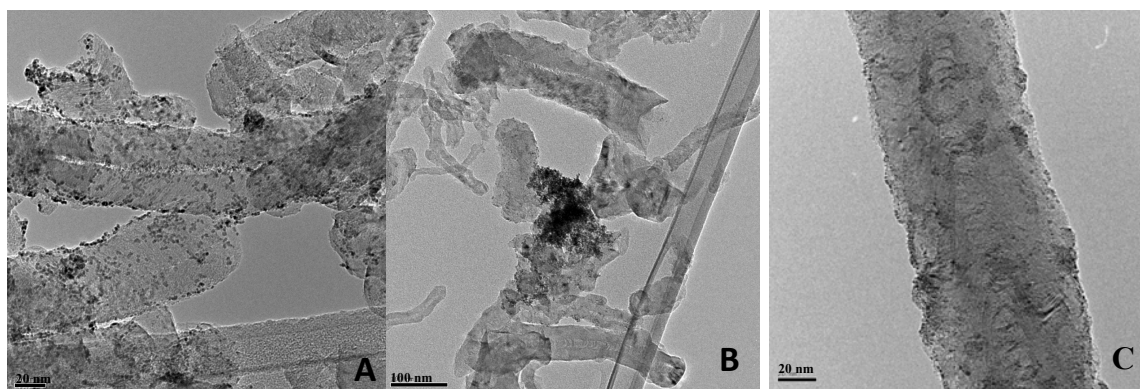
Figure 10. Current-time curves towards methanol oxidation at 0.45 V of fresh catalysts (**A**) and aged catalysts (**B**) in 2 M CH_3OH + 0.5 M H_2SO_4 at 25 °C. Current scale is normalized for the electroactive area estimated from CO_{ads} stripping voltammetry before each current time at 0.45 V. Adapted from Tsiouvaras *et al.* [43].
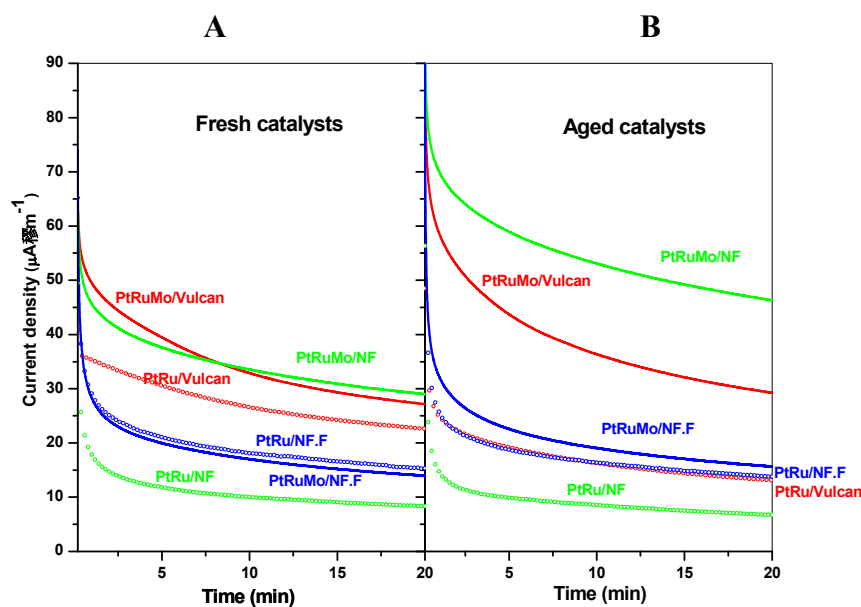
In order to study the activity and stability of the catalysts, current-time curves towards methanol oxidation were carried out at 0.45 V, 0.50 V, 0.60 V and again at 0.45 V. Figure 10 shows current-time dependence at 0.45 V of fresh catalyst and after electrochemical measurements (0.50 V and 0.60 V, not shown), denoted as aged catalysts. Fresh ternary PtRuMo/Vulcan and PtRuMo/NF catalysts exhibited higher activity than their binary counterparts. However, the incorporation of Mo to PtRu/NF.F did not improve the activity for methanol oxidation, even though binary catalyst supported on functionalized carbon nanofiber presented higher activity than PtRu supported on non-functionalized carbon nanofiber. This behavior can be explained taking into account that the functionalized carbon nanofiber hinders the stabilization of the electroactive MoO_x species. It is worth mentioning that after electrochemical measurements, the activity of the aged ternary catalysts increased markedly, especially in PtRu-MoO_x nanoparticles supported by non-functionalized carbon nanofiber (PtRuMo/NF), if

compared with the Mo free catalysts. In view of the fact that the activity towards methanol oxidation increases in ternary aged catalysts whereas decreases in binary aged catalysts, it appears that the role of Mo would be crucial for the activation of the electrocatalyst. The singular properties of carbon nanofibers as highly resistant to acid media and with good electrical and mechanical properties may play an important role in the activation and stabilization of the PtRuMo nanoparticles. These results point out the importance of the influence of the carbon support as well as its functionalization on the final activity of the electrocatalysts.

2.3. Effect of Composition

In the previous sections, it was examined the influence of the precursor in the synthesis, as well as the effect of thermal treatment in different environments (He or H_2) of PtRuMo/C catalysts. It was observed a beneficial effect towards CO and methanol oxidation reactions for all ternary catalysts. Nevertheless, the catalyst synthetized with the $(NH_4)_6Mo_7O_{24}.4H_2O$ precursor and treated with H_2 improves its performance towards both reactions in respect to the ternary catalysts treated either in He treatment or without thermal treatment. Therefore, the current subdivision is devoted to the study of the catalyst composition in the material thermally treated under a reductive atmosphere. Carbon monoxide, methanol and ethanol oxidation on PtRuMo/C catalysts in acidic media in a whole temperature range are studied to understand the mechanisms and kinetics involved [47].

The prepared catalysts record a nominal total metal loading of 30 wt%, and Pt:Ru:Mo atomic ratio of 1:1:0, 1:1:0.1 and 1:1:0.5 supported on carbon Vulcan XC 72R. The respective catalysts were designated as PR, 1MPR and 3MPR and the experimental data are shown in Table 4. The average particle sizes were close to 2.6 nm, regardless of the content of Mo. The X-ray diffractograms indicated the typical Pt fcc structure, apart from the 2θ values which all shifted to slightly higher values, due to the incorporation of Ru atoms into the Pt crystal lattice. The lattice parameter was also calculated in order to evaluate the level of PtRu alloying. The results pointed to a reduction in the Pt lattice parameter compared with pure Pt (3.923), which was perceived to be an improvement in Pt–Ru interaction. The XPS results established that the incorporation of Mo in 1MPR and 3MPR did not change the binding energy of the noble metals and confirms the presence of molybdenum oxide species, whose binding energy was assigned to Mo^{5+}. XPS analysis also showed that surface composition depends largely on the amount of Mo. 1MPR catalyst shows similar Pt:Ru:Mo surface composition to the metal loading of the bulk (Table 4). However, surface composition with higher amounts of Mo in 3MPR catalyst differs substantially from that of the bulk, with a lower surface amount of Pt. Therefore, Mo oxide species seem to block a small fraction of the Pt surface. As a consequence, 1MPR catalysts are more surface Pt-rich with respect to 3MPR catalyst, though they present similar amounts of Pt in the bulk.

Figure 11 shows the blank voltammetric profiles, in which the quasi-reversible peak at *ca.* 0.45 V is related to the oxidation/reduction of Mo oxide (Mo^{5+}) like species present in the catalyst surface [41,44,56]. As expected, the charge of this broad peak with onset at *ca.* 0.25 V increases with Mo loading and accordingly it is plausible an enhancement of water dissociation at very negative potentials (*i.e.*, lower than 0.25 V). Therefore, an enhanced tolerance towards carbon monoxide is expected [59].

Table 4. Effect of composition. Structural parameters of the samples.

| Catalysts	Bulk composition Pt:Ru (TXRF)	Average particle size (nm) (TEM)	Lattice parameter (fcc) (Å)	Metal loading (wt.%) [a] Pt:Ru:Mo	Surface metal loading (wt.%) (XPS) Pt:Ru:Mo
PR	1:0.7	2.6	3.899	21:8	17:11
1MPR	1:0.8:0.07	2.7	3.898	19:9:0.6	18:9:0.4
3MPR	1:0.8:0.3	2.6	3.894	18:7:3	12:8:3

[a] From TXRF and TG analysis.

Figure 11. Blank voltammograms recorded at PR, 1MPR and 3MPR catalysts at 30 °C in 0.5 M H_2SO_4. Sweep rate = 0.02 V s^{-1}. Reprinted with permission from *Int. J. Hydrogen Energ.* 2012, *37*, 7131 [47]. Copyright 2012. Elsevier.
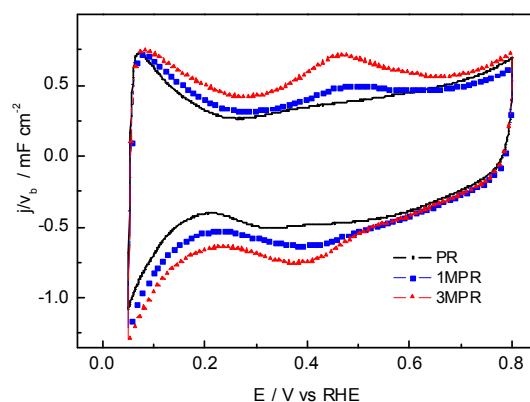
Figure 12. CO stripping record of PR, 1MPR and 3MPR catalysts at 20 °C (above) and 70 °C (below) in 0.5 M H_2SO_4. E_{ad} = 0.1 V, sweep rate = 0.02 V s^{-1}. Reprinted with permission from *Int. J. Hydrogen Energy* 2012, *37*, 7131 [47]. Copyright 2012. Elsevier.
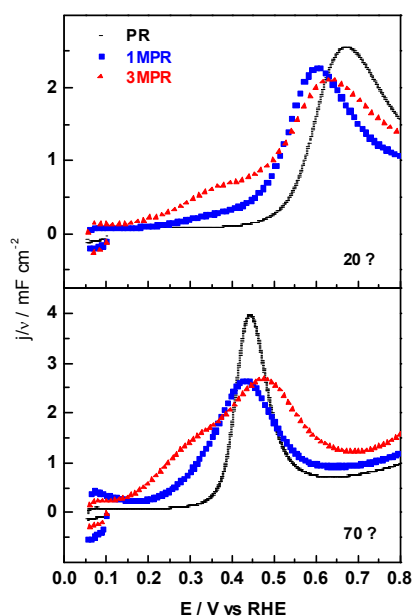
Figure 12 depicts the CO stripping voltammograms recorded at PR, 1MPR and 3MPR catalysts in sulphuric acid solution for two different temperatures (20 and 70 °C). A narrowing of the CO oxidation peaks with the rise of temperature is observed. Additionally, the binary catalysts develops only a single anodic peak, whereas ternary catalysts exhibits one main peak close to the binary peak and a shoulder (or pre-peak) at lower potential due to the presence of Mo. Also, it is notable that the pre-peak for the CO oxidation reaction (at $E \geq 0.1$ V) increases in intensity and shifts to lower potentials as the temperature and Mo percentage increase. Interestingly, the onset for CO_2 production shifts 0.2 V towards more negative potentials when a high concentration of Mo (PR5M) is introduced in the binary catalyst.

The most straightforward CO oxidation mechanism operating in these catalysts may be that proposed for the first time by Gilman [60]:

$$H_2O \rightleftarrows OH_{ad} + H^+ + e^- \tag{1}$$

$$CO_{ad} + OH_{ad} \rightleftarrows COOH_{ad} \tag{2}$$

$$COOH_{ad} \rightleftarrows CO_2 + H^+ + e^- \tag{3}$$

Therefore, the most plausible explanation for the enhancement in the catalytic activity towards CO oxidation with the introduction of a third metal (*i.e.*, Mo) may be related to an "easier" Mo oxidation, which provides oxygenated species at potentials as low as 0.1 V (Equation 1) [48]. In fact, enrichment of Mo oxide species on the surface with the rise of the temperature is in agreement with the observed increment in the CO tolerance. Thus, Mo seems to act as a promoter for the CO oxidation reaction.

Alcohol (methanol and ethanol) oxidation on binary and ternary catalysts was studied by voltammetry and chronoamperometry techniques across a whole temperature range ($30 \leq T \leq 70$ °C). The current transients were carried out from a potential step where the alcohol adsorption and oxidation are negligible ($E_i = 0.05$ V) to a potential similar to that achieved during operation conditions in a fuel cell ($E_f = 0.45$ and 0.5 V for methanol and ethanol, respectively).

As expected, the voltammetric analysis indicated that as the temperature was increased, the onset potentials for the oxidation of methanol and ethanol shifted negatively and the oxidation current increased for each catalyst. Also, it was observable a dependence of the catalytic activity towards the alcohol oxidation reaction with Mo content—*i.e.*, through the whole temperature range studied—an increment of Mo loading increases the current intensity during the alcohol oxidation reaction (not shown). Similar results were obtained through the chronoamperometry study, in which the highest performance towards methanol and ethanol oxidation was obtained at the 3MPR catalyst in all temperature ranges under study. Current-time curves for ethanol oxidation are shown in Figure 13.

The analysis of temperature effect is investigated through the Arrhenius plot (log j *vs.* 1/T) at 0.45 and 0.5 V for methanol and ethanol oxidation, respectively (Figure 14A,B). The data points were obtained from the current transients curves at 10 min, *i.e.*, at stationary current values. The slopes of the full traces give an estimation of the apparent activation energy (E_a) of the reaction as indicated in the figure. Since alcohol oxidation reaction has multiple side reactions (*i.e.*, CO, aldehyde, acid, *etc.*) and each one changes in a different way with the temperature, the apparent activation energy should be only used in a qualitative way, because it represents the overall reaction taking place during the alcohol oxidation.

Figure 13. Current-time curves for ethanol oxidation at 0.5 V *vs.* RHE recorded at PR, 1MPR and MPR catalysts at 30, 40, 50, 60 and 70 °C in 1 M CH$_3$CH$_2$OH + 0.5 M H$_2$SO$_4$. Reprinted with permission from *Int. J. Hydrogen Energy* 2012, *37*, 7131 [47]. Copyright 2012. Elsevier.
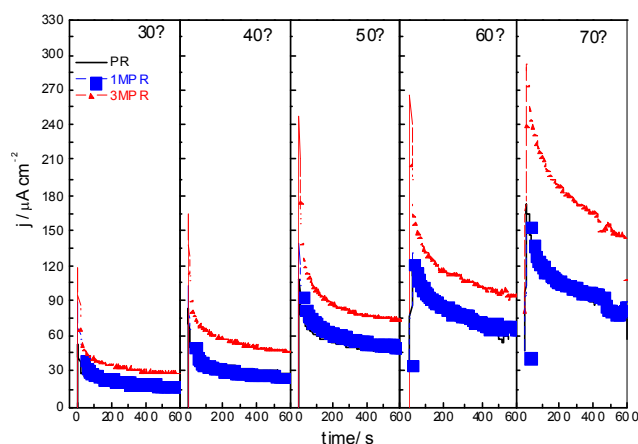
In this context, it is widely recognized that the structured fuel cell catalysts are characterized by unique properties endowed by the effect of spatial confinement of Pt sites because of the small particle size and strong contribution of the surface to the overall behavior [61]. In fact, it is well known that the kinetics of small organic molecules' oxidation on platinum depends on the structure of the material surface [62,63]. For example, three Pt neighboring atoms are necessary for carrying out the methanol oxidation reaction through the CO pathway, which is the principal catalyst poison [64]. On the other hand, The C-C bond cleavage of ethanol presents a considerable challenge that requires a significant overpotential and its rate is rather slow [65–68]. Additionally, one of the main prerequisited is a suitable catalyst surface for alcohol adsorption and dehydrogenation [68]. This step is central, since without it, the reaction of interest cannot be carried out.

Figure 14. Arrhenius plot and activation energies at 0.45 V for methanol oxidation (**A**) and at 0.5 V for ethanol oxidation (**B**) *vs.* RHE for PR, 1MPR and 3MPR catalysts. Reprinted with permission from *Int. J. Hydrogen Energy* 2012, *37*, 7131 [47]. Copyright 2012. Elsevier.
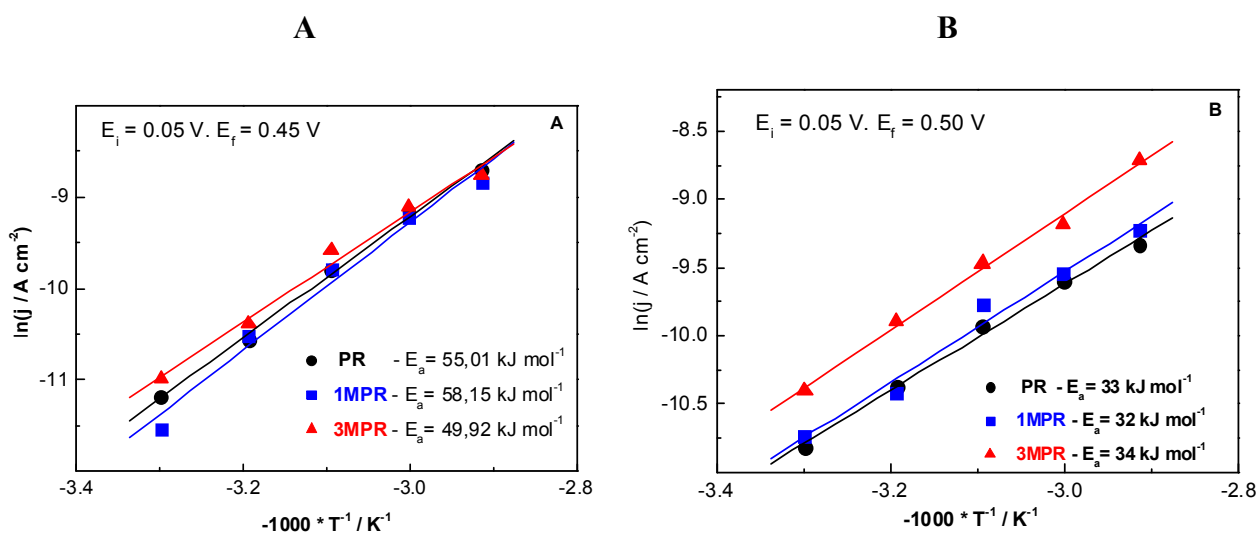
Returning to the apparent activation energy (E_a) obtained with methanol using ternary electrodes with those reported in the bibliography using PtRu alloys [69], we found that the values are similar, approximately 60 kJ mol^{-1}. Nevertheless, in a qualitative analysis, the slopes observed in the Figure 14A shows that the Ea slightly increases with a small introduction of Mo (1MPR) into the catalyst, but abruptly decreases when the Mo percentage increases (3MPR). The small Ea for the PR compared to the 1MPR is possibly due to the presence of a higher domain of crystallographic order at the binary catalyst, *i.e.*, small quantities of Mo in the catalyst possibly limits the dehydrogenation of methanol, which is in agreement with the fact that at low temperatures the dehydrogenation step is relevant (note that that at high temperatures the delivered currents are similar). However, the best catalyst for methanol oxidation is the 3MPR. This behavior may be related to a suitable surface structure, which provides a great amount of oxygenated species (-OH) at very low potentials (*ca.* 0.1 V *vs.* RHE) that liberate the surface from adsorbed CO, and consequently, the complete methanol oxidation reaction may be favored. It is important to note that surface composition is quite different to that of the bulk. In fact, it seems that Mo atoms are spread out at the bulk towards the surface, which in combination with Ru and Pt atoms, give an appropriate arrangement to carry out the methanol adsorption and oxidation reaction. This assumption is corroborated by CO oxidation studies performed above (Figure 12). The introduction of Mo into the binary catalyst enhances the water dissociation on the catalyst surface, and hence, the CO_2 formation. Therefore, the lower Ea observed at the 3MPR has to be associated to a facile CO removal by the synergetic effect of Mo. Consequently, similar current densities although with higher energetic efficiency are obtained with ternary rather than with binary catalysts.

On the other hand, the results obtained clearly show a promotional effect of Mo on PtRu catalysts for the electrooxidation of ethanol (Figure 13), which agrees perfectly with previous results [30,33,70]. The incorporation of different amounts of Mo over PtRu systems proves that the nature of the effect for ternary catalysts with similar structural characteristics, such as particle size and crystal phases, depends both on the surface amount of Mo and on the applied potential. Accordingly, chronoamperometric experiments have shown an increase in the current density with the Mo introduction during the ethanol oxidation at 0.5 V across the entire temperature range. At the same time, similar apparent activation energies were observed for all the catalysts (Figure 14B). Therefore, similar mechanisms are expected for ethanol oxidation operating in all catalysts. However, as was explained above, the apparent activation energy accounts for the set of the different reactions during the oxidation reaction. Consequently, it is not impossible to obtain an accurate idea of the governing mechanism during the ethanol oxidation on the present catalysts using just this kinetic parameter. However, diverse information can be extracted from the *in situ* spectroelectrochemical studies. In this way, an insight of the reactions occurring during the ethanol oxidation on binary and ternary catalysts can be acquired. In this sense, during the ethanol oxidation, DEMS and FTIRS experiments prove a decrease of CO and CO_2 formation and an increase of acetic acid (and acetaldehyde) with Mo introduction (Figure 15). Acetaldehyde either desorbs more readily as it is weakly held to the surface or reacts further via partial oxidation paths to form acetic acid. Therefore, the higher catalytic activity developed by the ternary catalysts during the ethanol oxidation has to be associated to an incomplete ethanol oxidation towards acetic acid formation. Additionally, the CO stripping study demonstrates an enhanced tolerance towards adsorbed CO on ternary catalysts. Therefore, it is can be stated that the higher current density delivered by the ternary catalysts is due to a fast replenishment and low

poisoning of the catalytic sites. In this way, similar apparent activation energy, but higher current densities are observed at the current transients.

Figure 15. *In situ* FTIR spectra recorded during ethanol electrooxidation on the PR, 1MPR and 3MPR catalysts in 0.1 M CH_3CH_2OH + 0.5 M $HClO_4$. Reprinted with permission from *Int. J. Hydrogen Energy* 2012, *37*, 7131 [47]. Copyright 2012. Elsevier.
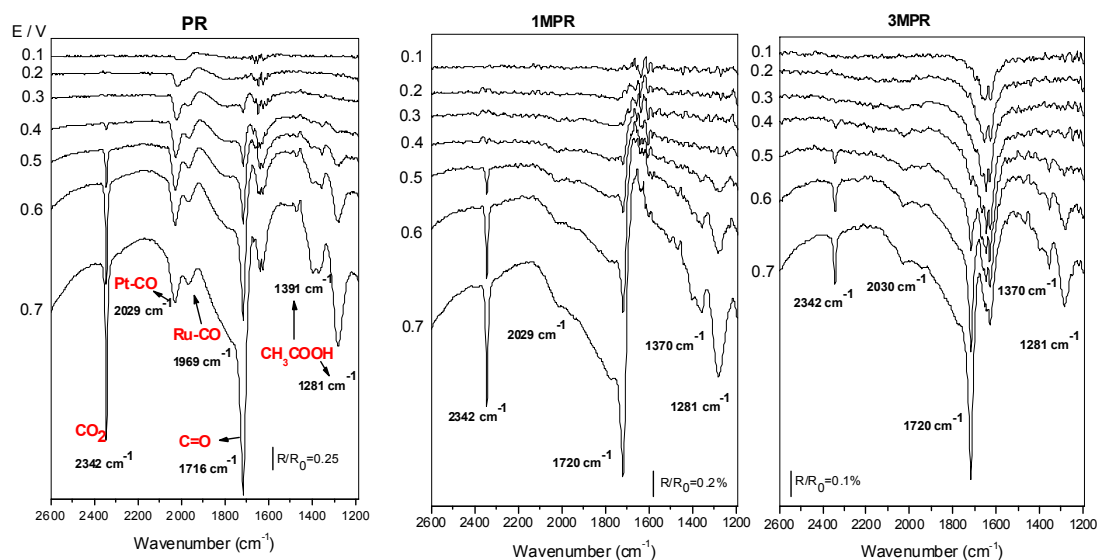
3. Experimental Section

3.1. Catalyst Preparation

PtRuMo nanoparticles deposited on carbon substrates were prepared following a new two-step procedure [41]. The first step in the synthesis consisted of the preparation of a MoO_x/C system. Hydrous molybdenum oxide was deposited on carbon substrate by the deposition-precipitation method [71]. First of all, carbon particles were dispersed in MeOH under vigorous stirring. The appropriate amount of Mo precursor was dissolved in de-ionized water (>18 MΩ/cm) to obtain a Mo solution, which was then added to the carbon dispersed solution and kept under vigorous stirring. Five equivalents of tetramethylammonium hydroxide solution were then added dropwise to precipitate the hydrous molybdenum oxide (MoO_xH_y) on the carbon particles. After 1h aging under stirring, the MoO_xH_y/C solid was recovered by filtration and dried at 110 °C for 17 h to obtain MoO_x/C. In a second step, platinum and ruthenium were loaded on the MoO_x/C sample according to the colloidal methodology [42]. The reaction was performed in water with aqueous solutions of reactants. The appropriate concentration of H_2PtCl_6 was reduced by adding a solution of $Na_2S_2O_5$ ($NaHSO_3$) to obtain a colorless soluble intermediate of platinum, which was then oxidized with H_2O_2 (30%, *v/v*). During the addition, the pH of the solution was adjusted to *ca.* 5 by adding Na_2CO_3. The appropriate amount of $RuCl_3$ solution was then added dropwise under continuous stirring while keeping the pH close to *ca.* 5. The required amount of carbon was added to the colloidal solution under constant stirring. Hydrogen gas was bubbled through this admixture for 2 h, and the suspension was allowed to settle, filtered, washed with hot

water and then dried in an air oven at 110 °C. Solutions were prepared using Millipore-MiliQ water and analytical-grade reagents. Four series of catalysts were prepared for our studies:

1. To study the effect of the Mo precursor [44], two ternary catalysts were prepared using $MoCl_5$ (Aldrich) and $(NH_4)_6Mo_7O_{24}$ (Aldrich) as precursors. Catalysts, with a nominal atomic ratio of Pt/Ru/Mo of 1/1/1, total metal loading of 30 wt.% and supported on Vulcan XC 72R, were labeled PRMCl and PRMNH, using $MoCl_5$ and $(NH_4)_6Mo_7O_{24}$, respectively. For comparison purpose, a binary catalyst PtRu (1:1)/C, labeled PR, was obtained following the same colloidal methodology.

2. To study the influence of thermal treatment [45], 30 wt.% PtRuMo (1:1:0.6)/Vulcan XC 72R catalyst (labeled PRM) was synthesized using $(NH_4)_6Mo_7O_{24}$ as Mo precursor. This catalyst was subjected to two thermal treatments: an aliquot part of the ternary catalyst was subjected to heating at 300 °C during 1 h in 50 cm^3 min^{-1} of 10% H_2/Ar (PRMH2); another aliquot of the ternary catalyst was heated at 300 °C for 1 h in He gas flow, 50 cm^3 min^{-1} (PRMHe). Commercially available electrocatalyst containing 30 wt% PtRu (1:1)/carbon (Johnson-Matthey), labeled PR/C (JM), and 20 wt.% Pt/carbon (ETEK), labeled Pt/C (ETEK) were used for comparison.

3. To study the effect of support [43], three supports were compared: Vulcan XC 72R, carbon nanofiber (NF) and carbon nanofiber functionalized with HNO_3 (NF.F). Six catalysts were synthesized, with three ternary PtRuMo (1:1:1) catalysts: PRM/Vulcan, PRM/NF and PRM/NF.F, and the respective binary PtRu (1:1) counterparts: PR/Vulcan, PR/NF and PR/NF.F.

4. To study the effect of composition [47], two ternary 30 wt.% PtRuMo catalysts supported on Vulcan XC 72R were prepared using $(NH_4)_6Mo_7O_{24}$ as Mo precursor and treated in H_2 at 300 °C for 1 h. Two different PtRuMo atomic ratios, 1:1:0.1 and 1:1:0.5, were investigated, and catalysts obtained were labeled as 1MPR and 3MPR, respectively.

3.2. Physicochemical Characterization

Atomic ratio Pt/Ru/Mo of samples was determined by total-reflection X-ray fluorescence (TXRF). Analysis was performed on a Seifert EXTRA-II spectrometer equipped with two X-ray fine focus lines, Mo and W anodes and a Si(Li) detector with an active area of 80 mm^2 and a resolution of 157 eV at 5.9 keV (MnKα). The Pt/Ru atomic ratio was determined using Pt*L*α and Ru*L*α emission lines in the XRF spectra after proper calibration with standard samples.

Thermogravimetric analysis (TGA) under controlled atmosphere was carried out on a Mettler Toledo TGA/SDTA851e using 200 cm^3 min^{-1} of N_2 as carrier gas, 20 cm^3 min^{-1} of oxygen as reactive gas, and a heating rate of 10 °C min^{-1}.

Metal phases and crystalline particle size have been determined using X-ray diffraction (XRD) measurements. XRD powder patterns were obtained on a PANalytical X'Pert Pro X-ray diffractometer using a Cu Kα source. The diffraction profiles of the samples were recorded within Bragg's angles ranging from 2°–90° at a scanning rate of 0.04° per s.

Particle size and morphology were evaluated from the transmission electron microscopy (TEM) images obtained in a JEM 2100F electron microscope operated with an accelerating voltage of 200 kV. The

standard procedure involved dispersing 4 mg of the sample in ethanol in an ultrasonic bath for 15 min. The sample was then placed on a Cu carbon grid where the liquid phase was evaporated.

The H_2 temperature-programmed reduction (H_2-TPR) experiments were run in a Micrometrics equipment model TPD/TPR 2900 fitted with a TCD detector. Samples of *ca.* 20 mg each were used. The TPR experiments were run in a 10% H_2/Ar stream, with a heating rate of 10 °C min^{-1} and 80 cm^3 min^{-1} flow rate.

X ray photoelectron spectroscopy (XPS) analysis was used in order to get information on the chemical state and concentration of surface species. XP spectra were obtained with a VG Escalab 200R spectrometer equipped with a hemispherical electron analyser (constant pass energy of 50 eV) and a MgKα (hν = 1254.6 eV) X-ray source, powered at 120 W. The XPS data signals were taken in increments of 0.1 eV with dwell times of 50 ms. Binding energies were calibrated relative to the C 1s peak at 284.6 eV. High resolution spectra envelopes were obtained by curve fitting synthetic peak components using the software *XPS peak*. The raw data were used with no preliminary smoothing. Symmetric Gaussian-Lorentzian product functions were used to approximate the line shapes of the fitting components.

3.3. Electrochemical Characterization

3.3.1. Three Electrode Electrochemical Cell

Electrochemical experiments were carried out in a thermostatted electrochemical cell using a three-electrode assembly at diverse temperature (20 < *T* < 70 °C) connected to an electrochemical analyzer (Autolab PGstat302N). A high surface area carbon rod was used as counter electrode and a reversible hydrogen electrode (RHE) in the supporting electrolyte was employed as a reference electrode. All potentials in the text are referencing this electrode. The working electrode was prepared by ultrasonically dispersing 2 mg of the electrocatalysts in 0.5 mL of pure water (Millipore) and 15 μL of Nafion. An aliquot of the dispersed suspension was pipetted on the top of the working electrode and dried at ambient temperature under argon atmosphere. The working electrodes were glassy carbon electrodes for CO$_{ad}$ stripping and current-transients experiments (3.0 mm diameter) and for differential electrochemical mass spectrometry (DEMS, 7.0 mm diameter) and an Au disk for Fourier transform infrared spectroscopy (FTIRS, 10 mm diameter). The experiments were carried out in 0.5 M sulphuric acid (Merck p.a.) and Milli-Q water (Millipore). First, the electrolyte was saturated with pure argon (99.998%, Air Liquide), and subsequently, ethanol (Merck) was added until a final concentration of 1 M was reached or bubbling CO gas (99.997%, Air Liquide). The oxidation of CO adsorbed was studied after bubbling the gas for 10 min while polarizing the electrode at 0.07 V, replacing CO by Ar bubbling, and a subsequent potential scan of up to 0.80 V. Current-time curves ethanol transients were obtained by stepping the potential from 0.05–0.50 V.

3.3.2. Electrochemical DMFC Cell Experiments

The cell employed was an experimental 1.1 cm^2 DMFC with stainless steel bipolar plates having serpentine flow channels. The Pt load in both anode and cathode was of 2 mg Pt/cm^2 and while the anodes used were homemade catalysts, the cathode was a 40 wt% Pt/C from ETEK$^®$. The catalysts

were sprayed onto carbon paper (120 Toray paper) and afterwards hot pressed to sandwich the Nafion$^\circledR$ 117 membrane. The cell was heated up to 75 °C and connected to an Autolab PGstat potentiostat.

Prior to the full cell experiments, all anodic catalysts were studied in half cell conditions. The anode flow was changed from H_2O to H_2O + CO or 2 M CH_3OH according to the study taking place, while the cathode flow is maintained at all times at 50 cm^3 H_2. At the half cell mode, the anode functions as a working electrode while the cathode as both a reference and counter electrode. Once the half-cell experiments concluded, the cathode flow was changed to synthetic air at 200 cm^3 min^{-1} and the anode flow was maintained at 3.5 cm^3 min^{-1} 2 M CH_3OH. At this point, fuel cell experiments commenced and the potentiostat, instead of applying potential, was limited to record the potential difference between the anode and the cathode according to the current flowing between them.

3.3.3. *In Situ* Spectroelectrochemical Techniques

FTIRS studies of the alcohol reaction were performed with a NICOLET 6700 FT-IR spectrometer equipped with a MCT detector and fitted with a PIKE Technologies VeeMAX II spectroscopic accessory. A poly (methyl methacrylate) (PMMA) cell with a 60 ° CaF_2 prism at its bottom was used. FTIR spectra were acquired from the average of 64 interferograms, obtained with 4 cm^{-1} resolution at selected potential, by applying 0.05 V single potential steps from a reference potential ($E_0 = 0.05$ V) in the positive direction up to 0.8 V. The reflectance ratio R/R_0 was calculated, where R and R_0 are the reflectances measured at the sample and the reference potential, respectively. In this way, positive and negative bands represent the loss and gain of species at the sampling potential, respectively.

Differential electrochemical mass spectrometry (DEMS) experiments were carried out in an electrochemical cell directly attached to the vacuum chamber of the mass spectrometer (Balzers QMG112) which uses a Faraday cup detector. Accordingly, gaseous species produced on the electroactive surface can be followed on-line by mass spectrometry. Volatile species generated at the electrode evaporate at the pores of the membrane into the vacuum and are detected by the mass spectrometer. Therefore, the experimental setup allows the simultaneous acquisition of mass spectrometric cyclic voltammograms (MSCVs) for selected masses and conventional voltammograms (CVs) recorded at a scan rate of 0.005 V s^{-1}.

4. Conclusions

The design, preparation and characterization of carbon-supported trimetallic electrocatalysts is an important part of the recent progress in fuel catalyst research. While there are still major challenges for achieving commercially viable catalysts with high activity, high stability, and low cost, fundamental insights have been gained into the control of size, shape, composition, and phase properties of the multimetallic catalysts. In this context, carbon-supports play a vital role in ascertaining the durability and cost of the electrocatalysts.

With the aim to solve the principal catalytic problem at the anode of low temperature fuel cells, the fundamental and applied study of carbon monoxide, methanol, ethanol, as well as water dissociation on novel carbon-supported PtRuMo electrocatalysts in acidic medium, was considered.

Accordingly, an extensive investigation was carried out on the synthesis and characterization of carbon-supported PtRuMo electrocatalysts. In this sense, the effect of the catalyst composition, Mo

precursor, carbon support and the influence of thermal treatment during the catalyst synthesis was deeply analyzed.

It was observed an important enhancement of the catalytic activity for CO, methanol and ethanol oxidation reactions when ternary catalysts were used. It is concluded that water dissociation is enhanced by the Mo presence in the catalyst, promoting the CO oxidation reaction. The latter also influences the performance towards methanol oxidation, and higher current density with a higher efficiency conversion was observed in the ternary catalysts. On the other hand, the higher current density delivered during ethanol oxidation reaction by the ternary catalysts is due to fast fuel replenishment and low poisoning of the catalytic sites. Though, an increment of by-side reactions such as acid and aldehyde that decrease the efficiency conversion was also observed.

Finally, the nature of the carbon support considerably affects the stabilization of MoO_x nanoparticles and also the performance in methanol electrooxidation. Accordingly, a significant increase of methanol oxidation was obtained in PtRuMoOx nanoparticles supported by non-functionalized carbon nanofiber, in parallel with a large reduction of the Pt amount in comparison with binary counterparts.

These results open a new area of investigation where combining the optimization of three-metal system composition and carbon support material, and increases in the efficiency of the electrocatalysts could be achieved.

Acknowledgments

Conflicts of Interest

The authors declare no conflict of interest.

References

1. Neergat, M.; Leveratto, D.; Stimming, U. Catalysts for direct methanol fuel cells. *Fuel Cells* **2002**, *2*, 25–30.
2. Demirci, U.B. Direct liquid-feed fuel cells: Thermodynamic and environmental concerns. *J. Power Sources* **2007**, *169*, 239–246.
3. Zhao, X.; Yin, M.; Ma, L.; Liang, L.; Liu, C.; Liao, J.; Lu, T.; Xing, W. Recent advances in catalysts for direct methanol fuel cells. *Energy Environ. Sci.* **2011**, *4*, 2736–2753.
4. Antolini, E. Catalysts for direct ethanol fuel cells. *J. Power Sources* **2007**, *170*, 1–12.
5. Petrii, O. PtRu electrocatalysts for fuel cells: A representative review. *J. Solid State Electrochem.* **2008**, *12*, 609–642.
6. De la Fuente, J.L.G.; Martínez-Huerta, M.V.; Rojas, S.; Hernández-Fernández, P.; Terreros, P.; Fierro, J.L.G.; Peña, M.A. Tailoring and structure of PtRu nanoparticles supported on functionalized carbon for DMFC applications: New evidence of the hydrous ruthenium oxide phase. *Appl. Catal. B* **2009**, *88*, 505–514.

7.   Alegre, C.; Calvillo, L.; Moliner, R.; González-Expósito, J.A.; Guill-Villafuerte, O.; Martínez-Huerta, M.V.; Pastor, E.; Lázaro, M.J. Pt and PtRu electrocatalysts supported on carbon xerogels for direct methanol fuel cells. *J. Power Sources* **2011**, *196*, 4226–4235.

8.   García, G.; Florez-Montaño, J.; Hernandez-Creus, A.; Pastor, E.; Planes, G.A. Methanol electrooxidation at mesoporous Pt and Pt-Ru electrodes: A comparative study with carbon supported materials. *J. Power Sources* **2011**, *196*, 2979–2986.

9.   Maiyalagan, T.; Alaje, T.O.; Scott, K. Highly Stable Pt-Ru Nanoparticles Supported on Three-Dimensional Cubic Ordered Mesoporous Carbon (Pt-Ru/CMK-8) as Promising Electrocatalysts for Methanol Oxidation. *J. Phys. Chem. C* **2011**, *116*, 2630–2638.

10. De la Fuente, J.L.G.; Martínez-Huerta, M.V.; Rojas, S.; Terreros, P.; Fierro, J.L.G.; Peña, M.A. Enhanced methanol electrooxidation activity of PtRu nanoparticles supported on H_2O_2-functionalized carbon black. *Carbon* **2005**, *43*, 3002–3005.

11. Antolini, E.; Gonzalez, E.R. A simple model to assess the contribution of alloyed and non-alloyed platinum and tin to the ethanol oxidation reaction on Pt-Sn/C catalysts: Application to direct ethanol fuel cell performance. *Electrochim. Acta* **2010**, *55*, 6485–6490.

12. Sieben, J.M.; Duarte, M.M.E. Nanostructured Pt and PtSn catalysts supported on oxidized carbon nanotubes for ethanol and ethylene glycol electro-oxidation. *Int. J. Hydrogen Energy* **2011**, *36*, 3313–3321.

13. Jiang, L.; Colmenares, L.; Jusys, Z.; Sun, G.Q.; Behm, R.J. Ethanol electrooxidation on novel carbon supported Pt/SnO$_x$/C catalysts with varied Pt:Sn ratio. *Electrochim. Acta* **2007**, *53*, 377–389.

14. Bambagioni, V.; Bianchini, C.; Marchionni, A.; Filippi, J.; Vizza, F.; Teddy, J.; Serp, P.; Zhiani, M. Pd and Pt-Ru anode electrocatalysts supported on multi-walled carbon nanotubes and their use in passive and active direct alcohol fuel cells with an anion-exchange membrane (alcohol = methanol, ethanol, glycerol). *J. Power Sources* **2009**, *190*, 241–251.

15. Chatterjee, M.; Chatterjee, A.; Ghosh, S.; Basumallick, I. Electro-oxidation of ethanol and ethylene glycol on carbon-supported nano-Pt and -PtRu catalyst in acid solution. *Electrochim. Acta* **2009**, *54*, 7299–7304.

16. Wang, M.Y.; Chen, J.H.; Fan, Z.; Tang, H.; Deng, G.H.; He, D.L.; Kuang, Y.F. Ethanol electro-oxidation with Pt and Pt-Ru catalysts supported on carbon nanotubes. *Carbon* **2004**, *42*, 3251–3272.

17. Koper, M.T.M.; Lukkien, J.J.; Jansen, A.P.J.; van Santen, R.A. Lattice gas model for CO electrooxidation on Pt-Ru bimetallic surfaces. *J. Phys. Chem. B* **1999**, *103*, 5522–5529.

18. Watanabe, M.; Motoo, S. Electrocatalysis by ad-atoms: Part II. Enhancement of the oxidation of methanol on platinum by ruthenium ad-atoms. *J. Electroanal. Chem.* **1975**, *60*, 267–273.

19. Iwasita, T. Electrocatalysis of methanol oxidation. *Electrochim. Acta* **2002**, *47*, 3663–3674.

20. Rabis, A.; Rodriguez, P.; Schmidt, T.J. Electrocatalysis for Polymer Electrolyte Fuel Cells: Recent Achievements and Future Challenges. *ACS Catal.* **2012**, *2*, 864–890.

21. Antolini, E. Carbon supports for low temperature fuel cell catalysts. *Appl. Catal. B* **2009**, *88*, 1–24.

22. Fei, Y.; Cao, X.; Yu, L.; Chen, S.; Lin, W. Synthesis and Catalytic Performance of PtRuMo Nanoparticles Supported on Graphene-Carbon Nanotubes Nanocomposites for Methanol Electro-Oxidation. *Int. J. Electrochem. Sci.* **2012**, *7*, 1251–1265.

23. Kakati, N.; Maiti, J.; Oh, J.Y.; Yoon, Y.S. Study of methanol oxidation of hydrothermally synthesized PtRuMo on multi wall carbon nanotubes. *Appl. Surf. Sci.* **2011**, *257*, 8433–8437.

24. Chen, S.; Ye, F.; Lin, W. Effect of operating conditions on the performance of a direct methanol fuel cell with PtRuMo/CNTs as anode catalyst. *Int. J. Hydrogen Energy* **2010**, *35*, 8225–8233.

25. Lee, K.R.; Jeon, M.K.; Woo, S.I. Composition optimization of PtRuM/C (M = Fe and Mo) catalysts for methanol electro-oxidation via combinatorial method. *Appl. Catal. B* **2009**, *91*, 428–433.

26. Wang, Z.B.; Zuo, P.J.; Yin, G.P. Investigations of compositions and performance of PtRuMo/C ternary catalysts for methanol electrooxidation. *Fuel Cells* **2009**, *2*, 106–113.

27. Morante-Catacora, T.Y.; Ishikawa, Y.; Cabrera, C.R. Sequential electrodeposition of Mo at Pt and PtRu methanol oxidation catalyst particles on HOPG surfaces. *J. Electroanal. Chem.* **2008**, *621*, 103–112.

28. Pasupathi, S.; Tricoli, V. Effect of third metal on the electrocatalytic activity of PtRu/Vulcan for methanol electro-oxidation. *J. Solid State Electrochem.* **2008**, *12*, 1093–1100.

29. Bauer, A.; Gyenge, E.L.; Oloman, C.W. Direct methanol fuel cell with extended reaction zone anode: PtRu and PtRuMo supported on graphite felt. *J. Power Sources* **2007**, *167*, 281–287.

30. Wang, Z.B.; Yin, G.P.; Lin, Y.G. Synthesis and characterization of PtRuMo/C nanoparticle electrocatalyst for direct ethanol fuel cell. *J. Power Sources* **2007**, *170*, 242–250.

31. Benker, N.; Roth, C.; Mazurek, M.; Fuess, H. Synthesis and characterization of ternary Pt/Ru/Mo catalysts for the anode of the PEM fuel cell. *J. New Mater. Electrochem. Syst.* **2006**, *9*, 121–126.

32. Hou, Z.; Yi, B.; Yu, H.; Lin, Z.; Zhang, H. CO tolerance electrocatalyst of PtRu-H_xMeO$_3$/C (Me = W, Mo) made by composite support method. *J. Power Sources* **2003**, *123*, 116–125.

33. Oliveira Neto, A.; Franco, E.G.; Arico, E.; Linardi, M.; Gonzalez, E.R. Electro-oxidation of methanol and ethanol on Pt-Ru/C and Pt-Ru-Mo/C electrocatalysts prepared by Bönnemann's method. *J. Eur. Ceramic Soc.* **2003**, *23*, 2987–2992.

34. Pinheiro, A.L.N.; Oliveira Neto, A.; de Souza, E.C.; Perez, J.; Paganin, V.A.; Ticianelli, E.; Gonzalez, E.R. Electrocatalysis on noble metal and noble metal alloys dispersed on high surface area carbon. *J. New Mater. Electrochem. Syst.* **2003**, *6*, 1–8.

35. Franco, E.G.; Neto, A.O.; Linardi, M.; Arico, E. Synthesis of electrocatalysts by the Bonnemann method for the oxidation of methanol and the mixture H$_2$/CO in a proton exchange membrane fuel cell. *J. Braz. Chem. Soc.* **2002**, *13*, 516–521.

36. Papageorgopoulos, D.C.; Keijzer, M.; de Bruijn, F.A. The inclusion of Mo, Nb and Ta in Pt and PtRu carbon supported 3electrocatalysts in the quest for improved CO tolerant PEMFC anodes. *Electrochim. Acta* **2002**, *48*, 197–204.

37. Götz, M.; Wendt, H. Bynary and ternary anode catalyst formulations including the elements W, Sn and Mo for PEMFCs operated on methanol or reformate gas. *Electrochim. Acta* **1998**, *43*, 3637–3644.

38. Anderson, A.B.; Grantscharova, E.; Seong, S. Systematic Theoretical Study of Alloys of Platinum for Enhanced Methanol Fuel Cell Performance. *J. Electrochem. Soc.* **1996**, *143*, 2075–2082.

39. Ji, Z.; Jalbout, A.F.; Li, J.Q. Adsorption and diffusion of OH on Mo modified Pt(111) surface: First-principles theory. *Solid State Commun.* **2007**, *142*, 148–153.

40. Horkans, J.; Shafer, M.W. Effect of orientation, composition and electronic factors in the reduction of O_2 on single crystal electrodes of the conducting oxides of molybdenum and tungsten. *J. Electrochem. Soc.* **1977**, *124*, 1196–1202.

41. Martínez-Huerta, M.V.; Rodríguez, J.L.; Tsiouvaras, N.; Peña, M.A.; Fierro, J.L.G.; Pastor, E. Novel synthesis method of CO-tolerant PtRu-MoO$_x$ nanoparticles: structural characteristics and performance for methanol electrooxidation. *Chem. Mater.* **2008**, *20*, 4249–4259.

42. Watanabe, M.; Uchida, M.; Motoo, S. Preparation of highly dispersed Pt + Ru clusters and the activity for the electrooxidation of methanol. *J. Electroanal. Chem.* **1987**, *229*, 395–406.

43. Tsiouvaras, N.; Martínez-Huerta, M.V.; Moliner, R.; Lázaro, M.J.; Rodríguez, J.L.; Pastor, E.; Peña, M.A.; Fierro, J.L.G. CO tolerant PtRu-MoO$_x$ nanoparticles supported on carbon nanofibers for direct methanol fuel cells. *J. Power Sources* **2009**, *186*, 299–304.

44. Tsiouvaras, N.; Peña, M.A.; Fierro, J.L.G.; Pastor, E.; Martínez-Huerta, M.V. The effect of the Mo precursor on the nanostructure and activity of PtRuMo electrocatalysts for Proton Exchange Membrane Fuel Cells. *Catal. Today* **2010**, *158*, 12–21.

45. Tsiouvaras, N.; Martínez-Huerta, M.V.; Paschos, O.; Stimming, U.; Fierro, J.L.G.; Peña, M.A. PtRuMo/C catalysts for direct methanol fuel cells: Effect of the pretreatment on the structural characteristics and methanol electrooxidation. *Int. J. Hydrogen Energy* **2010**, *35*, 11478–11488.

46. Martínez-Huerta, M.V.; Tsiouvaras, N.; Peña, M.A.; Fierro, J.L.G.; Rodriguez, J.L.; Pastor, E. Electrochemical activation of nanostructured carbon-supported PtRuMo electrocatalyst for methanol oxidation. *Electrochim. Acta* **2010**, *55*, 7634–7642.

47. García, G.; Tsiouvaras, N.; Pastor, E.; Peña, M.A.; Fierro, J.L.G.; Martínez-Huerta, M.V. Ethanol oxidation on PtRuMo/C catalysts: *In situ* FTIR spectroscopy and DEMS studies. *Int. J. Hydrogen Energy* **2012**, *37*, 7131–7140.

48. Alcaide, F.; Álvarez, G.; Tsiouvaras, N.; Peña, M.A.; Fierro, J.L.; Martínez-Huerta, M.V. Electrooxidation of H_2/CO on carbon-supported PtRu-MoO$_x$ nanoparticles for polymer electrolyte fuel cells. *Int. J. Hydrogen Energy* **2011**, *36*, 14590–14598.

49. Grgur, B.N.; Zhuang, G.; Markovic, N.M.; Ross, J.P.N. Electrooxidation of H_2/CO Mixtures on a Well-Characterized Pt$_{75}$Mo$_{25}$ Alloy Surface. *J. Phys. Chem. B* **1997**, *101*, 3910–3913.

50. Grgur, B.N.; Markovic, N.M.; Ross, P.N., Jr. Electrooxidation of H_2, CO and H_2/CO mixtures on a well-characterized Pt$_{70}$Mo$_{30}$ bulk alloy electrode. *J. Phys. Chem. B* **1998**, *102*, 2494–2501.

51. Holleman, A.F.; Wiberg, E. *Inorganic Chemistry*; Wiberg, N., Ed.; Academic Press: San Diego, CA, USA, 2001; pp. 1382–1402.

52. Briggs, D.; Seah, M.P. *Practical Surface Analysis by Auger and X-ray Photoelectron Spectroscopy*; Wiley: New York, NY, USA, 1990.

53. Hobbs, B.S.; Tseung, A.C.C. High performance, platinum activated tungsten oxide fuel cell electrodes. *Nature* **1969**, *222*, 556–558.

54. Bond, G.C.; Tripathi, J.B.P. Studies of Hydrogen Spillover. *J. Chem. Soc. Faraday Trans. 1* **1976**, *72*, 933–941.

55. Grgur, B.N.; Markovic, N.M.; Ross, P.N. The electrooxidation of H_2 and H_2/CO mixtures on carbon supported Pt$_x$Mo$_y$ alloy catalysts. *J. Electrochem. Soc.* **1999**, *146*, 1613–1619.

56. Mukerjee, S.; Urian, R.C. Bifunctionality in Pt alloy nanocluster electrocatalysts for enhanced methanol oxidation and CO tolerance in PEM fuel cells: Electrochemical and *in situ* synchrotron spectroscopy. *Electrochim. Acta* **2002**, *47*, 3219–3231.

57. Lebedeva, N.P.; Janssen, G.J.M. On the preparation and stability of bimetallic PtMo/C anodes for protno-exchange membrane fuel cells. *Electrochim. Acta* **2005**, *51*, 29–40.

58. Serp, P.; Corrias, M.; Kalck, P. Carbon nanotubes and nanofibers in catalysis. *Appl. Catalysis A* **2003**, *253*, 337–358.

59. García, G.; Koper, M.T.M. Carbon Monoxide Oxidation on Pt Single Crystal Electrodes: Understanding the Catalysis for Low Temperature Fuel Cells. *Chemphyschem* **2011**, *12*, 2064–2072.

60. Gilman, S. The Mechanism of Electrochemical Oxidation of Carbon Monoxide and Methanol on Platinum. II. The Reactant-Pair Mechanism for Electrochemical Oxidation of Carbon Monoxide and Methanol 1. *J. Phys. Chem.* **1964**, *68*, 70–80.

61. Arico, A.S.; Bruce, P.; Scrosati, B.; Tarascon, J.-M.; Schalkwijk, W.V. Nanostructured materials for advanced energy conversion and storage devices. *Nat. Mater.* **2005**, *4*, 366–377.

62. Hamnett, A. *Interfacial Electrochemistry; Theory, Experiment and Applications*; Wieckowski, A., Ed.; Marcell Dekker: New York, NY, USA, 1999; p. 843.

63. Sun, S.G.; Clavilier, J. Electrochemical study on the poisoning intermediate formed from methanol dissociation at low index and stepped platinum surfaces. *J. Electroanal. Chem.* **1987**, *236*, 95–112.

64. Cuesta, A. At Least Three Contiguous Atoms Are Necessary for CO Formation during Methanol Electrooxidation on Platinum. *J. Am. Chem. Soc.* **2006**, *128*, 13332–13333.

65. Camara, G.A.; Iwasita, T. Parallel pathways of ethanol oxidation: The effect of ethanol concentration. *J. Electroanal. Chem.* **2005**, *578*, 315–321.

66. Lamy, C.; Lima, A.; LeRhun, V.; Delime, F.; Coutanceau, C.; Leger, J.M. Recent advances in the development of direct alcohol fuel cells (DAFC). *J. Power Sources* **2002**, *105*, 283–296.

67. Colmenares, L.; Wang, H.; Jusys, Z.; Jiang, L.; Yan, S.; Sun, G.Q.; Behm, R.J. Ethanol oxidation on novel, carbon supported Pt alloy catalysts—Model studies under defined diffusion conditions. *Electrochim. Acta* **2006**, *52*, 221–233.

68. Neurock, M. Advances in Electrocatalysis, Materials, Diagnostics and Durability. In *First-Principles Modeling for the Electro-Oxidation of Small Molecules—Handbook of Fuel Cells—Fundamentals, Technology and Applications*; Vielstich, W., Lamm, A., Gasteiger, H.A., Eds.; Wiley: West Sussex, UK, 2009; Volume 5.

69. Zhu, J.; Cheng, F.; Tao, Z.; Chen, J. Electrocatalytic Methanol Oxidation of $Pt_{0.5}Ru_{0.5-x}Sn_x$/C (x = 0–0.5). *J. Phys. Chem. C* **2008**, *112*, 6337–6345.

70. Zhou, W.; Zhou, Z.; Song, S.; Li, W.; Sun, G.; Tsiakaras, P.; Xin, Q. Pt based anode catalysts for direct ethanol fuel cells. *Appl. Catal. B* **2003**, *46*, 273–285.

71. Ioroi, T.; Fujiwara, N.; Siroma, Z.; Yasuda, K.; Miyazaki, Y. Platinum and molybdenum oxide deposited carbon electrocatalyst for oxidation of hydrogen containing carbon monoxide. *Electrochem. Commun.* **2002**, *4*, 442–446.